Site-Specific One-To-One Click Coupling of Single Proteins to Individual Carbon Nanotubes: a Single-Molecule Approach

Mark Freeley,[†,^] Harley L. Worthy,[§,^] Rochelle Ahmed,[§] Ben Bowen,[§] Daniel Watkins,[§,#] J. Emyr Macdonald,[|] Ming Zheng,[‡] D. Dafydd Jones,[§,*] Matteo Palma[†,*]

[†] School of Biological and Chemical Sciences, Institute of Bioengineering, and Materials Research Institute, Queen Mary University of London, Mile End Road, London, E1 4NS, UK

[§] Division of Molecular Biosciences, School of Biosciences, Main Building, Cardiff University, Cardiff, CF10 3AX, Wales, UK

[|] School of Physics and Astronomy, Cardiff University, Queens's Building, The Parade, Cardiff CF24 3AA, U.K

[‡] Materials Science and Engineering Division, National Institute of Standards and Technology, 100 Bureau Drive, Gaithersburg, Maryland 20899-8542, United States

ABSTRACT: We report the site-specific coupling of single proteins to individual carbon nanotubes (CNTs) in solution and with single-molecule control. Using an orthogonal Click reaction, Green Fluorescent Protein (GFP) was engineered to contain a genetically encoded azide group and then bound to CNT ends in different configurations: in close proximity or at longer distances from the GFP's functional centre. Atomic force microscopy and fluorescence analysis in solution and on surfaces at the single-protein level confirmed the importance of bioengineering optimal protein attachment sites to achieve direct protein-nanotube communication and bridging.

INTRODUCTION

Here we present a facile strategy for the site-specific coupling of single proteins to individual carbon nanotubes, in solution and with single-molecule control. Proteins are nature's own nanomachines performing a wide variety of functions such as catalysis, charge transfer, energy conversion and molecular recognition. A central challenge in nanobiotechnology is the bottom-up assembly of platforms capable of monitoring and exploiting these biomolecular interactions with single-molecule sensitivity and control.[1-5] Probing the dynamics of single proteins/biomolecules can allow the measurement of distributions of molecular properties rather than their ensemble averages, and can offer unmatched sensitivity for a wide range of applications, from biosensing to molecular electronics.[3, 6-8]

In this regard, strategies that permit the interfacing of single biomolecules directly to nano-electronic systems are increasingly pursued for both fundamental biological studies, and for the fabrication of ultra-sensitive assays.[7-16] A key issue involved in the development of such platforms is related to the single-molecule control, and site-specific attachment, of the biomolecule of interest to the employed nanoelectrode. Additionally, an in-solution assembly strategy is highly desirable, towards the development of solution processable single-molecule bioelectronic systems and devices.

Among the approaches investigated so far, there has been great interest in the use of one-dimensional nanostructured materials as ideal nano-electronic systems for biological interfacing, and single walled carbon nanotubes (SWCNTs) emerged as strong candidates.[7-8, 17-19] It has been reported that target biomolecules, when in close proximity to SWCNTs, can alter the electronic properties of the nanotubes via various mechanisms, with even small changes to surface charge detectable.[6-8, 20] Moreover, SWCNTs are intrinsically the same size as biological moieties, ensuring appropriate size compatibility.

Interfacing biomolecules, predominantly nucleic acids, with SWCNTs has been accomplished *via* covalent[11, 21-23] and non-covalent chemical strategies,[24-27] and the interactions have been monitored via optical and electrical techniques.[7, 28-29] However, with regards to proteins, many of these approaches are non-specific in terms of attachment sites as well as optimal interface locations, and can result in uncontrolled multiple molecules adsorbed on an individual SWCNT. This in turn results in little scope for measuring individual proteins interfaced in defined orientations, and hampers the development of single-molecule biointerfaces for device implementation.

In this context, the importance of orientation and site-specific attachment has been demonstrated by Holland et al for glucose oxidase attached to a gold nanoparticle via different mutant residues,[30] while Della Pia et al showed how different orientations result in different single-molecule conductance for cytochrome b_{562}.[31] Nevertheless, the precise control, at the single-molecule level, over the number, positon and orientation of proteins[30-31] on nano-electronic systems such as carbon nanotubes, remains an unmet challenge.

In the study presented here, we directed the conjugation of single proteins selectively at the terminal ends of individual SWCNTs, for the in-solution assembly of monofunctionalized SWCNT-

protein heterostructures. As a proof of concept, two different CNT-protein configurations were investigated, where green fluorescent protein (GFP) mutants were engineered to exhibit CNT-anchoring residues either in close proximity (short axis, GFP^{SA}), or at larger distance (long axis, GFP^{LA}), from the GFP's functional center, the chromophore (CRO). To define the protein-SWCNT interaction, bio-orthogonal "1+1" Click chemistry[32] was used. Notably, fluorescence investigations in solution and on surfaces at the single-protein level, showed evidence of site-specific coupling between the SWCNTs and the GFPs, i.e. only the short axis bioengineered system exhibited the expected direct protein-nanotube communication.

RESULTS AND DISCUSSION

SWCNT Functionalization. We employed SWCNTs mildly sonicated and dispersed in water via DNA wrapping.[27] Single-stranded DNA tightly binds to the sidewalls of SWCNTs through π-π stacking, allowing for the dispersion of the nanotubes in aqueous solution; this further makes the SWCNTs compatible for their potential conjugation to biomolecules. Additionally, the DNA wrapping protects the sidewalls of the nanotubes leaving only the terminal end of the SWCNTs available for direct functionalization, via amidation reactions on the carboxylic acid groups present on the nanotubes termini.[33-35] This allowed us to covalently functionalize the terminal ends of our DNA-wrapped CNTs (ssDNA/SWCNT) with dibenzocyclooctyne (DBCO), employing established methods that we developed in previous works[33-35] (see also scheme S1).

DBCO-functionalized ssDNA/SWCNTs were then available to readily react with azide groups, in a copper-free ring strain promoted 1,3-dipolar cycloaddition (SPAAC).[32, 36-37] The superfolder version of green fluorescent protein (sfGFP)[38] was used to demonstrate the approach (see scheme 1) and the importance of linkage site on the protein-SWCNT communication: while GFPs are routinely used for their fluorescence properties (including Forster resonance energy transfer)[39-40] it is becoming more apparent that they also act as charge transfer proteins.[41-46]

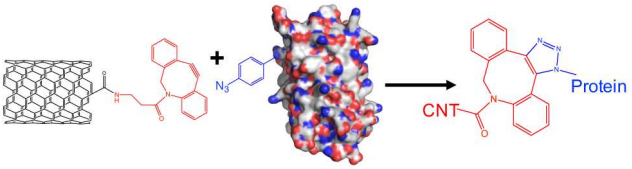

Scheme 1 Single protein attachment to SWCNTs: attachment process scheme.

We engineered two sfGFP variants to introduce an azide CNT-anchoring handle: using a reprogrammed genetic code[47] the non-canonical amino acid (ncAA) azF (*p*-azido-L-phenylalanine) can be incorporated at defined sites in a protein of interest in response to the TAG amber stop codon[48-49] (see scheme S2). To generate GFP^{SA} (Figure 1a), residue Gln204 that is in close proximity to the CRO (~16 Å estimated from CRO to DBCO-amine moiety) on the side of the barrel structure was substituted with azF. GFP^{LA} (Figure 1b) was constructed by replacing Glu132, which is further away (~35 Å) from the CRO at one end of the barrel, with azF. Mutation of residues Glu132 and Gln204 to azF has been shown previously to have minimal impact on GFP function, including when functionalised via SPAAC with DBCO moieties.[50] The two GFP mutants with modified residues allowed us to then form (in solution) ssDNA/SWCNT-GFP hybrids with specific protein orientations (see Figure 1a and 1b).

The covalent attachment of GFP^{SA} and GFP^{LA} mutants to DBCO-functionalized ssDNA/SWCNTs was monitored casting our hybrids' solutions on muscovite mica, and imaging the substrate surface via Atomic Force Microscopy (AFM). Figures 1c and 1d show representative images of GFP-SWCNT nanohybrids, where the proteins are tethered uniquely to the terminal ends of individual SWCNTs (see also the SI).

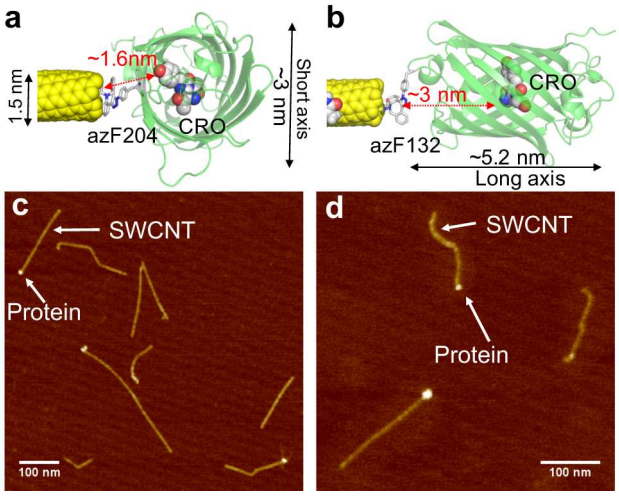

Figure 1 Schematics of the (a) short axis GFP^{204azF} (GFP^{SA}) and (b) long axis GFP^{132azF} (GFP^{LA}) CNT interface points and orientations: the chromophore (CRO) is shown as grey spheres, the DBCO-azF linkage sown as grey sticks and the CNT as gold spheres; the approximate triazole-CRO distance is highlighted in red. (c)AFM image of ssDNA/SWCNT-GFP^{SA} hybrids; d) AFM image of ssDNA/SWCNT-GFP^{LA} hybrids. Z-scales = 6nm

The AFM height profiles of GFPs and ssDNA/SWCNT-GFP hybrids correspond to the expected nanotube and proteins dimensions (see Figure 2). The two GFP mutants exhibited the same CNT linking efficiencies, of ca 30% as measured by AFM; moreover, AFM analysis revealed that among the nanohybrids obtained, 88% of SWCNT-GFP^{SA} heterostructures exhibited a single protein at only one end of the nanotube, while in the case of the SWCNT-GFP^{LA} nanohybrids the monofunctionalization yield obtained was 82%. Ratios of protein-SWCNTs greater than one (i.e. 2:1 protein-SWCNT hybrid formation, see Figure SI-1) were minimized thanks to the mild sonication process employed in the formation of DNA-wrapped CNTs[34, 51-52]: only a limited number of carboxylic groups, and hence DBCO protein anchoring sites, were present on the ssDNA/SWCNTs termini. Furthermore, the short nature of the DBCO linker assured close proximity between the protein and the nanotube, sterically hindering additional proteins from subsequent binding to the same nanotube terminal end.

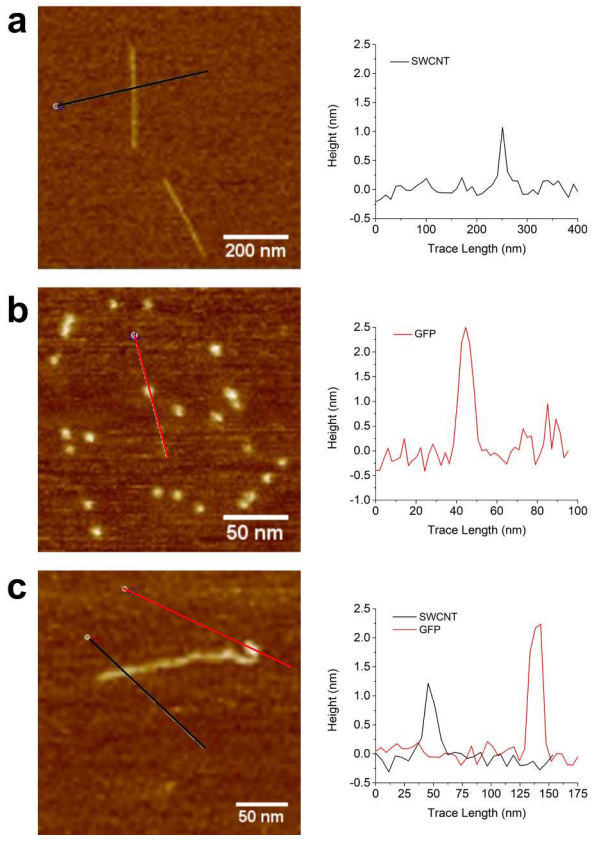

Figure 2 AFM images and corresponding height profiles for a) ssDNA/SWCNTs, b) individual GFP^{SA}, and c) SWCNT-GFP^{SA} hybrids. The same heights were observed in the case of GFP^{LA} and its hybrids. Z-scales= 6nm

Fluorescent Characterization. To demonstrate protein-CNT communication in our monofunctionalized nanohybrids, initially steady-state fluorescence spectroscopy was performed. GFPs have been shown to be able to act as light-induced electron donors in photochemical reactions with various electron acceptors,[43-44, 53] and changes in GFP fluorescence are a good indicator of communication, also through other coupled processes such as energy transfer.[54] Therefore, we compared sfGFPs' emission intensity before and after conjugation to ssDNA/SWCNTs keeping the protein concentration constant, and under identical processing conditions (see Figure 3 and the SI).

In the case of GFP^{SA} ~80% of the fluorescence emission was quenched in the monofunctionalized hybrid structures compared to the free protein. Control samples were measured where GFP^{SA} was conjugated to the linker only without nanotubes (Figure SI-2), and where ssDNA/SWCNT and GFP^{SA} were mixed in the absence of the linker molecule, i.e. without the formation of the protein-CNT heterostructures (Figure 3a). For both control experiments, only a limited quenching effect was observed (< 20%), indicating that the employed coupling strategy gives rise to an enhanced quenching beyond that caused by passive and transient physisorption of proteins and CNTs, or due to the chemical functionalization of the proteins at the bioengineered anchoring point. In comparison, fluorescence of GFP^{LA} in the long axis monofunctionalized hybrids was only quenched by ~20%, similar to that observed for simple mixing of GFP^{LA} and SWCNTs (Figure 3b and Figure SI-2b). (Additionally, fluorescence spectra of GFP in the presence and absence of DNA show that ssDNA had no effect on the fluorescent properties of either GFP variant: see figure SI-3). These results strongly suggest that direct electronic coupling between the proteins and the CNTs only occurs for the SWCNT-GFP^{SA} nanohybrids: the precise nature of the interface position plays an important role in the coupling due to the predicted shorter distance between the CRO and the nanotube in the GFP^{SA} hybrids compared to the GFP^{LA} heterostructures.

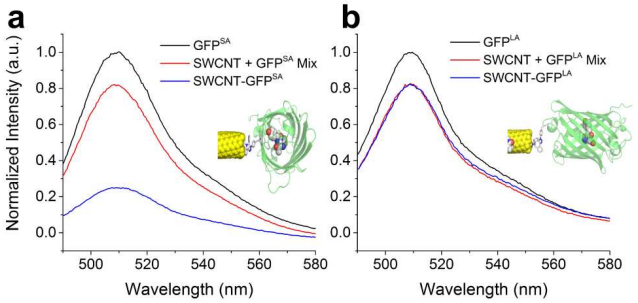

Figure 3 a) Steady-state fluorescence spectra of GFP^{SA} (black), SWCNT-GFP^{SA} hybrids (blue), and control sample where the protein and the nanotubes were mixed without the formation of heterostructures (red); b) Steady-state fluorescence spectra of GFP^{LA} (black), SWCNT-GFP^{LA} hybrids (blue), and control mixture (red).

Single-Molecule Fluorescence. In order to monitor GFP-nanotube coupling with single-molecule resolution, we cast dilute solutions of ssDNA/SWCNT-GFP hybrids and of unbound GFPs on glass coverslips to obtain physisorbed structures spaced at least 1 μm apart, hence optically resolvable. This allowed us to monitor, and compare, the fluorescence behavior of individual proteins and single nanohybrids via Total Internal Reflectance Fluorescence Microscopy (TIRF) (see Figure SI-4).

GFP has a characteristic blinking behavior which can be influenced by various processes (including its local environment).[55-57] A representative intensity vs time single-molecule trace for GFP^{SA}, showing "on" and off" states, can be seen in figure 4a, while the hybrid SWCNT- GFP^{SA} plot is shown in Figure 4b (see also Figure SI-5).

Single-molecule fluorescence dynamic studies of GFP have shown that off-time periods are independent of excitation intensity.[55] In our investigations, individual GFP^{SA} showed shorter off times, i.e. switching between "on" and "off" states, while the SWCNT-GFP^{SA} nanohybrids exhibited longer off time periods. This is a strong indication, at the single-molecule level, of direct coupling between the GFP^{SA} and the SWCNT in these short axis hybrids. In comparison, the SWCNT-GFP^{LA} heterostructures exhibited almost identical blinking rates when compared to the GFP^{LA} alone (see Figure SI-5).

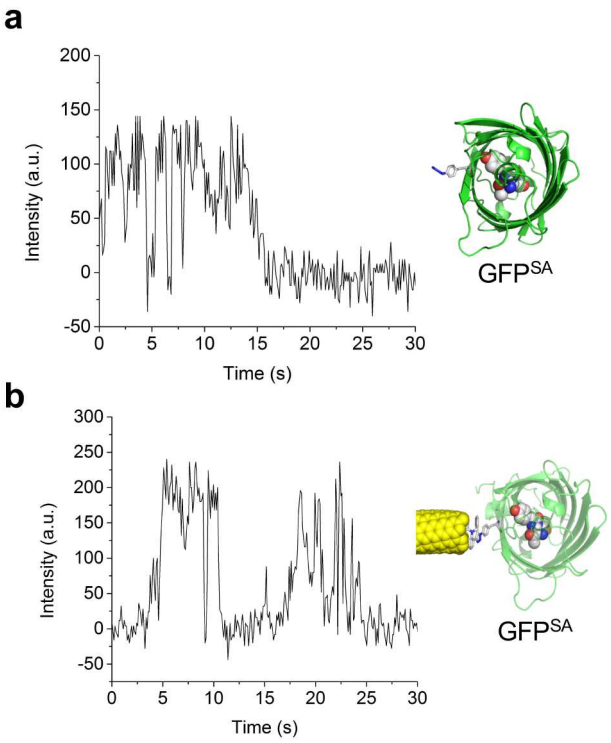

Figure 4 Representative single-molecule fluorescence traces for a) GFP^{SA}, and b) SWCNT-GFP^{SA} hybrid.

This behavior was confirmed and quantified by constructing histograms of single-molecule off-times for the hybrid structures and both sfGFP variants, as shown in Figure 5. The histograms were fitted with monoexponential decay curves as described in previous single-molecule GFP studies;[55-56] from these, the decay time for each sample was calculated. GFP^{SA} alone exhibited a decay time of 9.2 s, while the SWCNT-GFP^{SA} nanohybrids had a decay time of 7.7 s (Figure 5a). The shortening of the decay time corresponds to an increase in the length of off times, corroborating the longer off times seen in the intensity vs time plots displayed in figure 4.

In contrast, GFP^{LA} single-molecule off-events had a decay time of 6.6 s, which is unchanged in the SWCNT-GFP^{LA} hybrids (see Figure 5b). (A different decay time for the off events of GFP^{LA} compared to GFP^{SA} is to be expected: different mutants exhibit different blinking behaviour, as already observed in previous studies).[56,58] Thus, overall we only observed a change in the single-molecule optical properties of sfGFPs for the short axis SWCNT-GFP^{SA} nanohybrids. We believe this stems from the location of the CRO in relation to the site of CNT attachment, demonstrating the importance of appropriately designed linkage positions to functional communication.

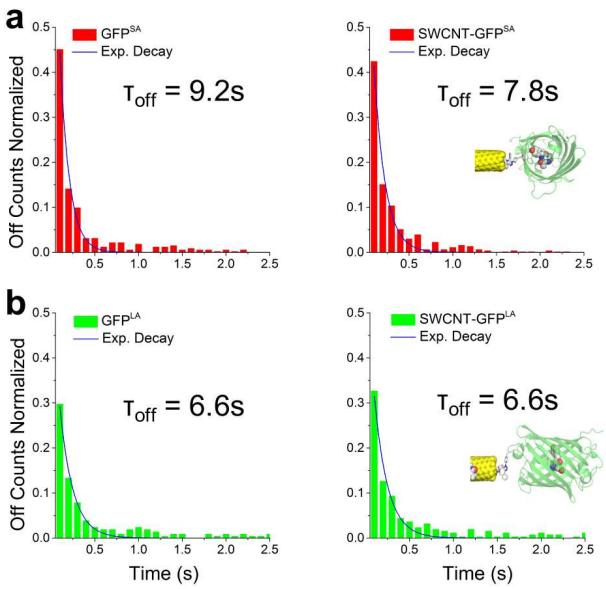

Figure 5 Histograms and exponential fits of the single-molecule off times of a) GFP^{SA} and SWCNT-GFP^{SA} hybrids, and b) GFP^{LA} and SWCNT-GFP^{LA} heterostructures.

In view of this, and of the relatively short distance between the CNT and the CRO in our GFPSA monofunctionalized heterostructures, the observed electronic coupling is likely to occur through energy or charge transfer. Energy transfer between GFP and a local acceptor can result in quenching in a distance dependent manner, as has been observed previously.[54,59] Additionally, photo-induced charge transfer between GFP, acting as the donor, [43-44, 53, 60] and the CNT as the acceptor[33, 35, 61-66] is a particularly interesting alternative to classical energy transfer given the differences between GFP^{SA} and GFP^{LA} in terms of the attachment position. GFP is known to act as an electron donor on photoexcitation, and as excitation is optimal for GFP, the CRO will dominate the photo-exited species. There is a known proton exit/entry point close to the attachment in GFP^{SA} (residue 204) linked to a charge transfer network back to CRO (Figure SI-6),[42, 67] and changes to these residues are known to affect the charge transfer network resulting in changes in the charged form of the CRO ground state.[39, 68] By and large, it is clear that in our short-axis nanohybrids the CNT and GFP are communicating, and thus the interface position with respect to the protein influences the degree of this coupling, where only the correctly bioengineered system exhibits the expected direct protein-nanotube communication.

Protein Junctions. Our protein-CNT assemblies further hold great potential for the development of solution processable single-molecule bioelectronic systems and devices (including gated GFP-based ones).[69-71] Biomolecular function (e.g. GFP electronic excitation [69-71,72]) can indeed be used to modulate conductance, and proteins have been observed to act as molecular gates.[31, 73-74] To facilitate such work, we engineered a sfGFP variant with two CNT-anchoring azide handles on opposite faces of the protein (Figure 6a). This would then allow us to control the assembly of sfGFP-SWCNT hybrids where a single protein could bridge two nanotube segments, which can then act as potential nanoelectrodes. The additional azF ncAA was incorporated in place of Glu111 on the opposite face of the barrel to residue 204 (Figure 6a) so generating the GFP^{SAx2} variant. Recombinant production GFP^{SAx2} by a double

TAG suppression was successful generating a functional, fluorescent (Figure SI-7). The bio-orthogonal nature of the SPAAC reaction means that no protein-protein or SWCNT-SWCNT can form, thus leading to the formation of a SWCNT-sfGFP-SWCNT construct by design. Figure 6b shows a characteristic AFM image of the typical 1:2 protein-SWCNT junctions obtained, while AFM images height profiles are displayed in Figure SI-8. Further investigations in our laboratories will focus on optimizing the yield of formation of such systems and investigating their electrical properties in device configurations, taking advantage of the single-molecule knowledge developed in the study presented here.

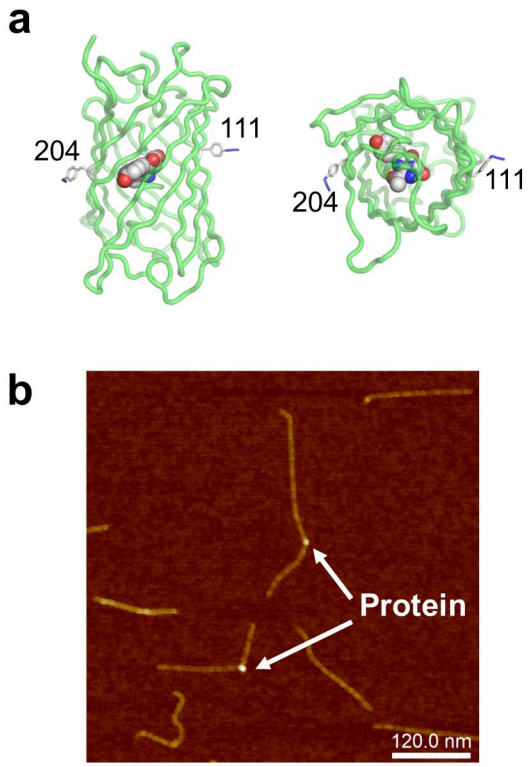

Figure 6 a) Proposed model (top-down and side-on views) of the GFP^{SAx2} variant with residues 111 and 204 mutated to azF *in silico;* b) AFM image of SWCNT-GFP^{SAx2}-SWCNT junctions. Z-scales = 6 nm.

CONCLUSION

In summary, we have presented, to the best of our knowledge, the first example of controlled covalent attachment and coupling of single proteins to individual SWCNTs via an in-solution methodology. A monofunctionalization yield of more than 80% was obtained in the formation of ssDNA/SWCNT-GFP heterostructures with controlled protein orientation. Fluorescence investigations showed evidence of site-specific functional communication between the proteins and the nanotubes. Additionally, single molecule fluorescence studies confirmed the importance of bioengineering optimal protein attachment sites: evidence of coupling was observed when sfGFP was attached via the 204 residue, close to the chromophore, while in the case of sfGFP attached via the 132 residue, which is at a larger distance from the chromophore, no protein communication with the nanotube was detected. Finally, the incorporation of two bioorthogonal reaction handles into individual sfGFPs allowed the construction of single protein bridging systems. As ncAA incorporation with bio-orthgonal reaction handles becomes more accessible[47,75], including azF,[76] our approach provides a general route for protein attachment to the ends of carbon nanotubes. By and large, we presented a powerful approach to generate tailored and optimal single protein-CNT hybrids that hold great potential for the development of solution-processable single-molecule bioelectronic systems and devices based on the use of carbon nanoelectrodes.

METHODS AND MATERIALS

SWCNT Wrapping. SWCNTs were wrapped with DNA and dispersed in water according to published procedures.[77] Generally, 1mg of HiPco nanotube was suspended in 1ml aqueous DNA (Integrated DNA Technologies) solution (1mg/ml DNA; 0.1M NaCl), and was sonicated in an ice water bath for 90 minutes at a power of 3W (Sonics, VC130PB). After sonication, samples were separated into 0.1ml aliquots and centrifuged for 90 minutes at 16000g (Eppendorf 5415C), which precipitated only insoluble material. The supernatant, containing DNA-dispersed SWCNTs at a mass concentration in the range of 0.2 to 0.4 mg/ml, was collected and purified by size exclusion chromatography giving segments of a defined length at a concentration of 40μg/ml.[78-79]

Production of sfGFP variants containing azF. Incorporation of p-azido-L-phenylalanine (azF) into sfGFP was achieved using the pDULE-cyanoRS plasmid [80] in which the non-canonical amino acid (ncAA) was incorporated in response to an introduced TAG amber stop codon. The gene encoding sfGFP was present with the pBAD backbone plasmid [49-50]. The variants GFP^{LA} (codon for residue Glu132 mutated to azF) and GFP^{SA} (codon for residue Gln204 mutated to TAG) have been reported previously [50]. The double azF variant $sfGFP^{SAx2}$ (codons for residues Glu111 and Gln204 mutated to TAG) was produced using the Site-directed ligase-independent mutagenesis (SLIM) procedure as described in Chiu *et al* (2004) [81] with primers shown in Table S1 and the plasmid housing the GFP^{SA} as the template. The final DNA sequence of the gene encoding the double sfGFP variant (as determined by Sanger sequencing) is given in the supporting information.

E. coli One Shot ® TOP10 Electrocomp™ cells (Thermo Fisher) were co-transformed with pBAD-sfGFP and pDULE-cyanoRS plasmids. Transformed cells were used to inoculate 100 mL of arabinose autoinduction media according to the Studier *et al.* [82] recipe and supplemented with carbenicillin and tetracycline (final concentration 50 μg/mL and 25 μg/mL respectively). Cultures were left overnight at 37°C in a shaking incubator. Each expression was done in duplicate. One hour after induction, p-azido-L-phenylalanine dissolved in 1 M NaOH was added to a final concentration of 1 mM to one culture whilst and equivalent volume of 1M NaOH was added to the second culture to act as a negative control. The cultures were then incubated for a further 20 hr in the dark (to prevent photolysis of azF). After incubation 1 mL samples were taken to measure the OD_{600} of cultures and to analyse whole cell expression. These 1mL samples were centrifuged at 15,000 xg for 5 mins and resuspended in SDS loading buffer to an equivalent OD_{600} of 10. SDS-PAGE showed successful production of protein in only the +ve azF sample (Figure SI-6d). The remaining cells from the positive sample were harvested by centrifugation at 5000 xg for 20 minutes. Pellets were resuspended in 10 mL of 50 mM Tris-HCl (pH 8.0) and 300 mM NaCL, containing 1mM PMSF and lysed via French press at 1250 psi. Cell lysates were then clarified by centrifugation at 25,000 xg for 30-60 minutes. All purification steps of sfGFP variants were performed using an ÄKTAprime plus FPLC system (GE Healthcare). Firstly, using a HiTrap™ Talon® Crude column (GE Healthcare) equilibrated in 50 mM Tris HCl (pH 8.0), 300 mM NaCl with 20 mM imidazole. Bound protein was then eluted in a single step of 250 mM imidazole into a single 5 mL fraction. The eluted fraction was then loaded onto a HiLoad™ Superdex™ 200 pg (26/600, GE Healthcare) equilibrated in 50 mM Tris-HCL (pH 8.0). All purification and subsequent storage was in the dark to prevent photolysis of the phenyl azide group.

SWCNT Functionalization. SWCNTs (6.25ug/ml) were mixed in a 1:1 ratio with MES buffer (0.2M; pH 4.7; ThermoScientific) containing 1-

ethyl-3-[3-dimethylaminopropyl]carbodiimide hydrochloride (EDC; 4mM; Sigma Aldrich) and N-hydroxysulfosuccinimide (sulfo-NHS; 10mM; Sigma Aldrich). The solution was shaken at room temperature (R.T.) for 30 minutes, then Dulbecco's phosphate buffered saline, purchased from Thermo Scientific, was added in a 1:1 ratio. A DPBS solution of dibenzocyclooctyne-amine (DBCO-amine; 2uM; Sigma Aldrich) was added in a tenth of the total reaction volume giving a final molecule concentration of 200nM. The solution was shaken at R.T. overnight. Excess linker was removed by dialysis against DPBS using Slide-A-Lyzer™ MINI Dialysis Devices with a 20kDa cutoff purchased from Thermo Scientific.

To conjugate GFP to SWCNTs, GFP (1uM) was added to freshly dialysed SWCNT-cyclooctyne solution to give a final concentration of 200nM. The reaction was shaken overnight at R.T. and free GFP was removed with Amicon Ultra 100kDa centrifugal filters purchased from Millipore in a centrifuge at 13000rpm for 2 minutes three times, replacing the buffer with DPBS each time.

Atomic Force Microscopy. SWCNT-GFP conjugates were first characterized by atomic force microscopy (AFM) with a Bruker Dimension Icon. AFM samples were prepared by cleaving mica with sticky tape three times and an aqueous solution of $MgSO_4$ (100ul; 1M) was cast on the mica's surface. This was washed off with tissue and blown dry with compressed air. SWCNT-GFP conjugate solutions (5ul) were cast on the mica in a 12-well plate, which were then covered with parafilm and shaken at R.T. for 20 minutes. The mica was rinsed with water and blown dry with compressed air. Samples were imaged with a Bruker Dimension Icon atomic force microscope with ScanAsyst Air tips. Samples were prepared immediately before AFM imaging. Yield of attachment was determined by analyzing over 100 ssDNA/SWCNTs per hybrid sample (multiple samples were prepared,) and counting the number of nanotubes with and without GFP on their termini. The GFP on the terminal ends of CNTs could be distinguished by a greater height as measured by AFM topographical profiles (at least 2 nm compared to the ca 1nm height of the CNTs). We captured multiple AFM images, typically of a 4 x 4 μm size, and counted the CNTs present. This was done for each set of samples at different locations on the substrate surface, in order to get full representation

Steady-State Fluorescence Spectroscopy. SWCNTs were functionalized with DBCO-amine as described above. For the GFP attachment, the GFP concentration was kept constant at 25nM, and no filtration step followed the reaction between the SWCNT and GFP. Fluorescence spectra were collected on an Agilent Cary Eclipse Fluorescence Spectrometer.

Single-Molecule Fluorescence Characterization. For single-molecule fluorescence microscopy measurements, glass coverslips were arranged on a Teflon rack and cleaned in piranha solution (3:1 mixture of sulfuric acid to hydrogen peroxide) for 1 minute. The Teflon rack was then transferred to a solution of MilliQ water for 10 minutes, before being rinsed with acetone and ethanol. Finally, the coverslips were blown dry with compressed air. The SWCNT-GFP conjugates were deposited on the glass coverslips using the same method as the mica deposition. The coverslips were then fixed to glass slides and imaged with a Zeiss super resolution LSM 710 ELYRA PS.1 in TIRF (total internal reflection fluorescence) mode. An excitation wavelength of 488nm was used. Time series of each sample were taken with an exposure time of 100 milliseconds for 60 seconds. ImageJ was used to plot emission intensity of single GFPs against time (see figure 4 and SI-5). OriginLab9 and Matlab were used to measure "off" event lengths and build the histograms of single-molecule events, where the number of events is plotted against the length of the off event. 25 proteins per sample were analyzed for the single-molecule experiments and histograms were constructed with a binning width of 100 milliseconds. The counts in each bin were normalized by dividing the bin by the total number of events observed in a given sample set. Histograms were fitted with monoexponential decays, from which the decay constant was obtained.

ASSOCIATED CONTENT

Supporting Information. Additional experimental procedures, protein engineering, AFM images, steady-state fluorescence, fluorescence microscopy and data analysis.

The Supporting Information is available free of charge on the ACS Publications website.

AUTHOR INFORMATION

Corresponding Author

*m.palma@qmul.ac.uk; * JonesDD@cardiff.ac.uk

Present Addresses

#School of Biochemistry, University Walk, Bristol BS8 1TD UK

Author Contributions

^ These authors contributed equally.

Funding Sources

No competing financial interests have been declared.

ACKNOWLEDGMENT

We gratefully acknowledge financial support from the Air Force Office of Scientific Research under Award FA9550-16-1-0345. We thank Clayton Rabideau for helpful discussions. DDJ would like to thank the BBSRC (BB/H003746/1 and BB/M000249/1), EPSRC (EP/J015318/1) and Cardiff SynBio Initiative/SynBioCite for supporting this work. HW with a Cardiff University BBSRC-facing studentship and BB with a BBSRC SWBio DTP studentship.

REFERENCES

1. Min, W.; English, B. P.; Luo, G. B.; Cherayil, B. J.; Kou, S. C.; Xie, X. S., *Acc Chem Res* **2005,** *38*, 923-931.
2. Claridge, S. A.; Schwartz, J. J.; Weiss, P. S., *ACS Nano* **2011,** *5*, 693-729.
3. Ishijima, A.; Yanagida, T., *Trends Biochem Sci* **2001,** *26*, 438-444.
4. Ritort, F., *J Phys-Cond Mat* **2006,** *18*, R531-R583.
5. Smiley, R. D.; Hammes, G. G., *Chem Rev* **2006,** *106*, 3080-3094.
6. Choi, Y.; Moody, I. S.; Sims, P. C.; Hunt, S. R.; Corso, B. L.; Perez, I.; Weiss, G. A.; Collins, P. G., *Science* **2012,** *335*, 319-24.
7. Guo, X., *Adv Mater* **2013,** *25*, 3397-408.
8. Rosenstein, J. K.; Lemay, S. G.; Shepard, K. L., *Wiley Interdiscip Rev Nanomed Nanobiotechnol* **2015,** *7*, 475-93.
9. Guo, X.; Small, J. P.; Klare, J. E.; Wang, Y.; Purewal, M. S.; Tam, I. W.; Hong, B. H.; Caldwell, R.; Huang, L.; O'Brien, S.; Yan, J.; Breslow, R.; Wind, S. J.; Hone, J.; Kim, P.; Nuckolls, C., *Science* **2006,** *311*, 356-359.
10. Liu, S.; Zhang, X.; Luo, W.; Wang, Z.; Guo, X.; Steigerwald, M. L.; Fang, X., *Angew Chem Int Ed Engl* **2011,** *50*, 2496-502.
11. Guo, X.; Gorodetsky, A. A.; Hone, J.; Barton, J. K.; Nuckolls, C., *Nat Nano* **2008,** *3*, 163-167.
12. Wang, H.; Muren, N. B.; Ordinario, D.; Gorodetsky, A. A.; Barton, J. K.; Nuckolls, C., *Chem Sci* **2012,** *3*, 62-65.
13. Wen, J.; Xu, Y.; Li, H.; Lu, A.; Sun, S., *Chem Commun (Camb)* **2015,** *51*, 11346-58.
14. Willner, I.; Willner, B., *Trends Biotechnol* **2001,** *19*, 222-30.

15. De Leo, F.; Magistrato, A.; Bonifazi, D., *Chem Soc Rev* **2015,** *44*, 6916-53.
16. Zhang, A. Q.; Lieber, C. M., *Chem Rev* **2016,** *116*, 215-257.
17. Sorgenfrei, S.; Chiu, C. Y.; Gonzalez, R. L.; Yu, Y. J.; Kim, P.; Nuckolls, C.; Shepard, K. L., *Nat Nano* **2011,** *6*, 125-131.
18. So, H. M.; Won, K.; Kim, Y. H.; Kim, B. K.; Ryu, B. H.; Na, P. S.; Kim, H.; Lee, J. O., *J Am Chem Soc* **2005,** *127*, 11906-11907.
19. Ordinario, D. D.; Burke, A. M.; Phan, L.; Jocson, J. M.; Wang, H. F.; Dickson, M. N.; Gorodetsky, A. A., *Analyt Chem* **2014,** *86*, 8628-8633.
20. Sims, P. C.; Moody, I. S.; Choi, Y.; Dong, C.; Iftikhar, M.; Corso, B. L.; Gul, O. T.; Collins, P. G.; Weiss, G. A., *J Am Chem Soc* **2013,** *135*, 7861-8.
21. Tan, B.; Hodak, M.; Lu, W.; Bernholc, J., *Phys Rev B* **2015,** *92*.
22. Vedala, H.; Roy, S.; Doud, M.; Mathee, K.; Hwang, S.; Jeon, M.; Choi, W., *Nanotechnology* **2008,** *19*, 265704.
23. Weizmann, Y.; Chenoweth, D. M.; Swager, T. M., *J Am Chem Soc* **2011,** *133*, 3238-41.
24. Ito, M.; Ito, Y.; Nii, D.; Kato, H.; Umemura, K.; Homma, Y., *J Phys Chem C* **2015,** *119*, 21141-21145.
25. Lyonnais, S.; Goux-Capes, L.; Escude, C.; Cote, D.; Filoramo, A.; Bourgoin, J. P., *Small* **2008,** *4*, 442-6.
26. Nepal, D.; Geckeler, K. E., *Small* **2007,** *3*, 1259-65.
27. Tu, X.; Manohar, S.; Jagota, A.; Zheng, M., *Nature* **2009,** *460*, 250-3.
28. Landry, M. P.; Ando, H.; Chen, A. Y.; Cao, J. C.; Kottadiel, V. I.; Chio, L.; Yang, D.; Dong, J. Y.; Lu, T. K.; Strano, M. S., *Nat Nano* **2017,** *12*, 368-377.
29. Budhathold-Uprety, J.; Langenbacher, R. E.; Jena, P. V.; Roxbury, D.; Heller, D. A., *ACS Nano* **2017,** *11*, 3875-3882.
30. Holland, J. T.; Lau, C.; Brozik, S.; Atanassov, P.; Banta, S., *J Am Chem Soc* **2011,** *133*, 19262-5.
31. Della Pia, E. A.; Macdonald, J. E.; Elliott, M.; Jones, D. D., *Small* **2012,** *8*, 2341-4.
32. Sletten, E. M.; Bertozzi, C. R., *Acc Chem Res* **2011,** *44*, 666-676.
33. Attanzio, A.; Sapelkin, A.; Gesuele, F.; van der Zande, A.; Gillin, W. P.; Zheng, M.; Palma, M., *Small* **2017,** *13*, 1603042
34. Palma, M.; Wang, W.; Penzo, E.; Brathwaite, J.; Zheng, M.; Hone, J.; Nuckolls, C.; Wind, S. J., *J Am Chem Soc* **2013,** *135*, 8440-3.
35. Zhu, J.; McMorrow, J.; Crespo-Otero, R.; Ao, G.; Zheng, M.; Gillin, W. P.; Palma, M., *J Am Chem Soc* **2016,** *138*, 2905-8.
36. Hartley, A. M.; Zaki, A. J.; McGarrity, A. R.; Robert-Ansart, C.; Moskalenko, A. V.; Jones, G. F.; Craciun, M. F.; Russo, S.; Elliott, M.; Macdonald, J. E.; Jones, D. D., *Chem Sci* **2015,** *6*, 3712-17.
37. Jewett, J. C.; Sletten, E. M.; Bertozzi, C. R., *J Am Chem Soc* **2010,** *132*, 3688-90.
38. Pedelacq, J. D.; Cabantous, S.; Tran, T.; Terwilliger, T. C.; Waldo, G. S., *Nat biotech* **2006,** *24*, 79-88.
39. Tsien, R. Y., *Annu Rev of Biochem* **1998,** *67*, 509-44.
40. Shaner, N. C.; Steinbach, P. A.; Tsien, R. Y., *Nat Methods* **2005,** *2*, 905-9.
41. Remington, S. J., *Protein Sci* **2011,** *20*, 1509-19.
42. van Thor, J. J., *Chem Soc Rev* **2009,** *38*, 2935-50.
43. Bogdanov, A. M.; Mishin, A. S.; Yampolsky, I. V.; Belousov, V. V.; Chudakov, D. M.; Subach, F. V.; Verkhusha, V. V.; Lukyanov, S.; Lukyanov, K. A., *Nat Chem Bio* **2009,** *5*, 459-461.
44. Lv, X.; Yu, Y.; Zhou, M.; Hu, C.; Gao, F.; Li, J.; Liu, X.; Deng, K.; Zheng, P.; Gong, W.; Xia, A.; Wang, J., *J Am Chem Soc* **2015,** *137*, 7270-3.
45. Shinobu, A.; Palm, G. J.; Schierbeek, A. J.; Agmon, N., *J Am Chem Soc* **2010,** *132*, 11093-102.
46. Shinobu, A.; Agmon, N., *J Chem Theory Comput* **2017,** *13*, 353-369.
47. Liu, C. C.; Schultz, P. G., *Annu Rev of Biochem* **2010,** *79*, 413-44.
48. Chin, J.; Santoro, S.; Martin, A.; King, D.; Wang, L.; Schultz, P., *J Am Chem Soc* **2002,** *124*, 9026-7.
49. Reddington, S. C.; Rizkallah, P. J.; Watson, P. D.; Pearson, R.; Tippmann, E. M.; Jones, D. D., *Angew Chem Int Ed Engl* **2013,** *52*, 5974-7.
50. Reddington, S. C.; Tippmann, E. M.; Jones, D. D., *Chem Commun* **2012,** *48*, 8419-21.
51. Kaempgen, M.; Lebert, M.; Haluska, M.; Nicoloso, N.; Roth, S., *Adv Mater* **2008,** *20*, 616-620.
52. Riesz, P.; Kondo, T., *Free Rad Biol Med* **1992,** *13*, 247-270.
53. Choi, J.-W.; Nam, Y.-S.; Choi, H.-G.; Lee, W. H.; Kim, D.; Fujihira, M., *Synth Met* **2002,** *126*, 159-163.
54. Arpino, J. A.; Czapinska, H.; Piasecka, A.; Edwards, W. R.; Barker, P.; Gajda, M. J.; Bochtler, M.; Jones, D. D., *J Am Chem Soc* **2012,** *134*, 13632-40.
55. Garcia-Parajo, M. F.; Segers-Nolten, G. M. J.; Veerman, J.-A.; Greve, J.; van Hulst, N. F., *PNAS* **2000,** *97*, 7237-7242.
56. Dickson, R. M.; Cubitt, A. B.; Tsien, R. Y.; Moerner, W. E., *Nature* **1997,** *388*, 355-8.
57. Acharya, A.; Bogdanov, A. M.; Grigorenko, B. L.; Bravaya, K. B.; Nemukhin, A. V.; Lukyanov, K. A.; Krylov, A. I., *Chem Rev* **2017,** *117*, 758-795.
58. Peterman, E. J. G.; Brasselet, S.; Moerner, W. E., *J Phys Chem A* **1999,** *103*, 10553-10560.
59. Ganesan, S.; Ameer-beg, S. M.; Ng, T. T. C.; Vojnovic, B.; Wouters, F. S., *PNAS* **2006,** *103*, 4089-4094.
60. Acikgoz, S.; Ulusu, Y.; Akin, S.; Sonmezoglu, S.; Gokce, I.; Inci, M. N., *Ceram Inte* **2014,** *40*, 2943-2951.
61. Li, C.; Xia, J.; Wang, Q.; Chen, J.; Li, C.; Lei, W.; Zhang, X., *ACS Appl Mat Int* **2013,** *5*, 7400-7404.
62. Hu, L.; Zhao, Y. L.; Ryu, K.; Zhou, C.; Stoddart, J. F.; Grüner, G., *Adv Mater* **2008,** *20*, 939-946.
63. Jeong, S.; Shim, H. C.; Kim, S.; Han, C.-S., *ACS Nano* **2010,** *4*, 324-330.
64. Hao, F.; Dong, P.; Zhang, J.; Zhang, Y.; Loya, P. E.; Hauge, R. H.; Li, J.; Lou, J.; Lin, H., *Sci Rep* **2012,** *2*, 368.
65. Batmunkh, M.; Biggs, M. J.; Shapter, J. G., *Small* **2015,** *11*, 2963-2989.
66. Sheeney-Haj-Ichia, L.; Basnar, B.; Willner, I., *Angew Chem Inte Ed* **2005,** *44*, 78-83.
67. Salna, B.; Benabbas, A.; Sage, J. T.; van Thor, J.; Champion, P. M., *Nat Chem* **2016,** *8*, 874-80.
68. Pakhomov, A. A.; Martynov, V. I., *Chem & Bio* **2008,** *15*, 755-64.
69. Choi, J.-W.; Nam, Y.-S.; Oh, B.-K.; Lee, W. H.; Fujihira, M., *Synth Met* **2001,** *117*, 241-243.
70. Lee, B.; Takeda, S.; Nakajima, K.; Noh, J.; Choi, J.; Hara, M.; Nagamune, T., *Biosensors and Bioelectronics* **2004,** *19*, 1169-1174.
71. Choi, J.-W.; Nam, Y. S.; Jeong, S.-C.; Lee, W. H.; Petty, M. C., *Curr Appl Phys* **2006,** *6*, 839-843.
72. Korpany, K. V.; Langat, P.; Kim, D. M.; Edelman, N.; Cooper, D. R.; Nadeau, J.; Blum, A. S., *J Am Chem Soc* **2012,** *134*, 16119-22.
73. Della Pia, E. A.; Chi, Q.; Macdonald, J. E.; Ulstrup, J.; Jones, D. D.; Elliott, M., *Nanoscale* **2012,** *4*, 7106-13.
74. Artes, J. M.; Diez-Perez, I.; Gorostiza, P., *Nano Lett* **2012,** *12*, 2679-84.
75. Lang, K.; Chin, J. W., *Chem Rev* **2014,** *114*, 4764-4806.
76. Reddington, S.; Watson, P.; Rizkallah, P.; Tippmann, E.; Jones, D. D., *Biochem Soc Trans* **2013,** *41*, 1177-1182.
77. Zheng, M.; Jagota, A.; Semke, E. D.; Diner, B. A.; McLean, R. S.; Lustig, S. R.; Richardson, R. E.; Tassi, N. G., *Nat Mater* **2003,** *2*, 338-342.
78. Huang, X.; McLean, R. S.; Zheng, M., *Analyt Chem* **2005,** *77*, 6225-6228.
79. Khripin, C. Y.; Tu, X.; Howarter, J.; Fagan, J.; Zheng, M., *Analyt Chem* **2012,** *84*, 8733-8739.
80. Miyake-Stoner, S. J.; Refakis, C. A.; Hammill, J. T.; Lusic, H.; Hazen, J. L.; Deiters, A.; Mehl, R. A., *Biochem* **2010,** *49*, 1667-77.
81. Chiu, J.; March, P. E.; Lee, R.; Tillett, D., *Nucleic Acids Res* **2004,** *32*, e174.
82. Studier, F. W., *Prot Expr Puri* **2005,** *41*, 207-34.

Table of Contents artwork